Journal of Zhejiang University-SCIENCE A (Applied Physics & Engineering) 2023 24(7):569-583
www.jzus.zju.edu.cn; www.springer.com/journal/11582
E-mail: jzus_a@zju.edu.cn

Research Article

https://doi.org/10.1631/jzus.A2200446

Check for updates

Monotonic uplift behavior of anchored pier foundations in soil overlying rock

Yizhou SUN[1], Honglei SUN[2]✉, Chong TANG[3], Yuanqiang CAI[2], Feng PAN[4]

[1]*College of Civil Engineering and Architecture, Zhejiang University, Hangzhou 310058, China*
[2]*College of Civil Engineering, Zhejiang University of Technology, Hangzhou 310014, China*
[3]*State Key Laboratory of Coastal and Offshore Engineering, Dalian University of Technology, Dalian 116024, China*
[4]*Zhejiang Electric Power Design Institute Co. Ltd., China Energy Engineering Group, Hangzhou 310012, China*

Abstract: Rock-embedded foundations with good uplift and bearing capacity are often used in mountains or hilly areas. However, there are soil layers with a certain thickness on the rocks in these mountainous areas, and the utilization of those soil layers is a problem worthy of attention in foundation construction. Considering construction- and cost-related factors, traditional single-form foundations built on such sites often cannot provide sufficient resistance against uplift. Therefore, an anchored pier foundation composed of anchors and belled piers, specifically constructed for such conditions, can be invaluable in practice. This paper introduces an experimental and analytical study to investigate the uplift capacity and the uplift mobilization coefficients (UMCs) of the anchored pier foundation. In this study, three in-situ monotonic pullout tests were carried out to analyze the load–displacement characteristics, axial force distribution, load transfer mechanism, and failure mechanism. A hyperbolic model is used to fit the load–displacement curves and to reveal the asynchrony of the ultimate limit states (ULSs) of the anchor group and the belled pier. Based on the results, the uplift capacity can be calculated by the UMCs and the anchor group and pier uplift capacities. Finally, combined with the estimation of the deformation modulus of the soil and rock, the verification calculation of the uplift capacity and UMC was carried out on the test results from different anchored pier foundations.

Key words: Uplift capacity; Anchored pier foundation; Belled pier; Rock anchor; Uplift mobilization coefficient (UMC)

1 Introduction

Piers and rock anchors are widely used forms of uplift resistant foundations (Park et al., 2013; Harris and Madabhushi, 2015). Piers are used in areas with deep soils and rock anchors are used in areas with exposed rock or rock with thin overburden.

The southern part of Zhejiang Province, China, is dominated by hills and mountains, and the rocks in these areas are generally covered with a thickness of soil (Ma et al., 2015). Pier foundations are difficult to use in such areas with thin soils, and usually the bottom of the foundation needs to be embedded in the rock to ensure uplift capacity. The deeply buried pier foundation usually needs to be embedded in the bedrock, which is difficult to excavate (Kulhawy, 2015). However, if rock anchors are chosen for such sites, the soil layer needs to be removed. This means an increase in excavation and a waste of the bearing capacity of the in-situ soil.

An anchored pier foundation consists of a pier and rock anchors (Cheng et al., 2012; Jia et al., 2014; Sun et al., 2022). A foundation constructed in this way exhibits high stiffness and pullout resistance due to the pier being embedded in the in-situ soil and the rock anchors. Fig. 1 shows the different shapes of the anchored pier foundations. However, as far as we know, research has yet to be conducted on the monotonic uplift capacity and failure mechanism of anchored piers. The monotonic uplift capacity and the load distribution are the objects of research on the uplift behavior of anchored piers. Results of field tests conducted on three anchored piers, subjected to monotonic uplift, are presented here. The load–displacement (P-s) curves were fitted using a hyperbolic model

✉ Honglei SUN, sunhonglei@zju.edu.cn
Yizhou SUN, https://orcid.org/0000-0002-2553-352X

Received Sept. 24, 2022; Revision accepted Dec. 29, 2022;
Crosschecked Apr. 24, 2023

© Zhejiang University Press 2023

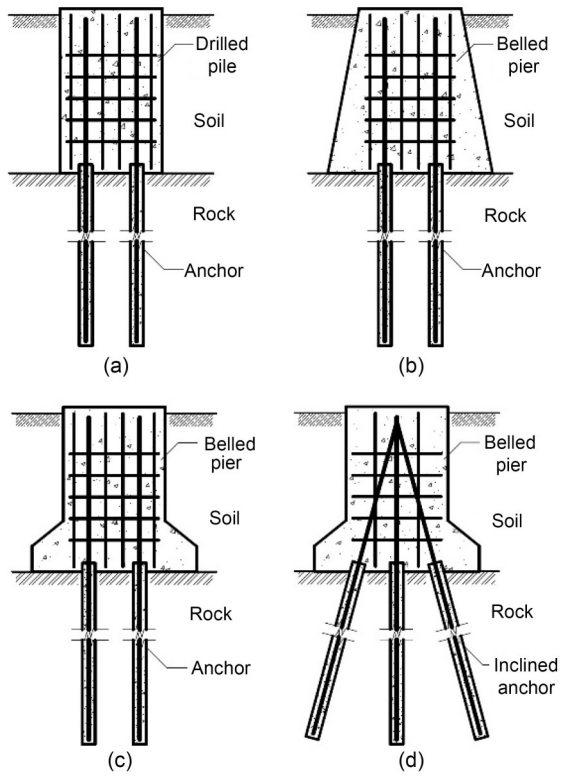

Fig. 1 Examples for the anchored piers: (a) anchored pile foundation; (b) anchored pier foundation (cap); (c) anchored pier foundation (belled pier); (d) anchored pier foundation (inclined anchor)

based on the analysis of load distribution and failure mechanisms. The calculation method for the uplift capacity of anchored piers is proposed based on the uplift mobilization coefficient (UMC) concept and the current design framework. The verification calculation was carried out on the uplift test results of anchored pier foundations with different geological conditions and geometric dimensions. Combined with the estimation method of geotechnical deformation modulus, the parameter determination method in UMC calculation was supplemented and refined.

Generally, the uplift capacity of the upper pier of the anchored pier depends on the shear capacity of the undisturbed soil. Previous studies have established the failure mechanism and the methods used to determine the uplift capacity of belled piers (Meyerhof and Adams, 1968; Wang et al., 2011; Li et al., 2022; Wu et al., 2022; Zhang et al., 2022). Honda et al. (2011) proposed a theoretical solution to predict the uplift capacity of belled piles in dense sand. Qian et al. (2015) conducted pullout tests of 41 full-scale belled piers in Gobi gravel and analyzed the uplift load–displacement curves. Four representative uplift interpretation criteria were used to evaluate the capacity of each belled pier and the interrelationships of these criteria were established. Understanding the failure mechanism of the pier foundation is essential for research into load-transfer characteristics, design, and engineering applications. The primary failure mechanism of belled piers under tensile loads has been reviewed by Pacheco et al. (2008). According to these studies, there are two failure modes of belled piles: shallow foundation failure and deep foundation failure.

The pullout resistance and failure mechanism of anchors have also been extensively studied. The uplift capacity calculation and design of anchors can be obtained from specifications (IEEE, 2001; BSI, 2013). Serrano and Olalla (1999) proposed a set of equations to describe the failure mechanism of anchors and calculated the uplift capacity by analyzing the force balance of the anchor on the fracture surface at the ultimate limit state (ULS). In that study, they also proposed to classify the anchor failure shape into "short anchors" and "long anchors" according to the slenderness ratio and rock mass parameter. Numerous studies have used laboratory and field tests, complemented by analytical and numerical analyses, to investigate the anchoring mechanism (Ma et al., 2016; Fabris et al., 2021). Kim and Cho (2012) categorized the failure modes of anchors into four groups: tensile failure of the steel tendon, shear failure at the tendon–grout interface, shear failure at the grout–rock interface, and shaped failure of the rock. Zhang et al. (2019) employed the classification method proposed by Serrano and Olalla (1999) to divide the failure modes of anchors into three types: slipping destruction, monolithic destruction, and compound destruction.

2 Field investigation of anchored pier foundations

2.1 Background and construction process

The site of the field tests for the present study was in Yeshanlong in Qingtian County, Lishui City, Southern Zhejiang Province, China. The geology was investigated, including a survey and geotechnical sampling. Uplift tests were conducted sequentially on three anchored pier foundations; the loading was static and monotonous. No groundwater was found at the test site. The view of the site is shown in Fig. 2.

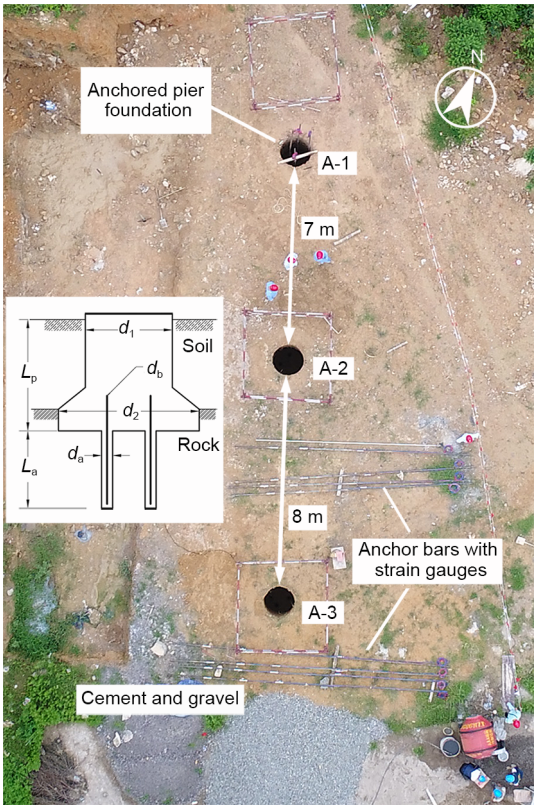

Fig. 2 Top view of the test site

The dimensions of the foundation are shown in Table 1, where L_p and L_a are the lengths of the piers and anchors, and d_1, d_2, d_a, and d_b are the diameters of the column of the pier, the diameter of the belled bottom, the diameter of the anchor hole, and the diameter of the anchor bar, respectively. Considering the pull-out synchronization of the anchors and avoiding the group effect, all the foundations were uniformly distributed with four anchors. The space between the anchors was 0.5 m. Anchor lengths of 1, 2, and 3 m were chosen to ensure that there was a significant difference in the uplift capacity of the anchor group, no plastic damage to the material at the ULS of the foundation, and that construction quality was assured.

In the first step, a suitable construction area was selected based on project requirements and geological profile (Fig. 3a). A geological survey and sample testing were carried out to determine the suitability of the anchored pier design and site layout plan in the area (Fig. 3b). Once the center point of the foundation was determined, the belled piers were excavated and formed using hand tools (Fig. 3c). The surrounding soil was not affected during excavation and construction, so the sidewalls remained rough. Drilling was started once the pier pit was checked and accepted. The drill rod was extended into the pit with the drilling machine positioned in the design location (Fig. 3d). The diameters of the boreholes and anchor bolts were 120 and 40 mm, respectively. All anchor bolts were threaded steel bars with a design strength of 400 MPa (design tensile force was 502.7 kN). At the same time, strain gauges were connected to the bolts through sleeves (Fig. 3e). Both the strain gauge and the sleeve had a design tensile strength of 500 MPa to ensure that they would not be damaged before the steel bar. After the boreholes were formed, the bolts and sensors were inserted and installed (Fig. 3f), and the grouting material was then poured into the boreholes. The grouting material was a fine aggregate concrete with a compressive strength of 35 MPa under standard curing conditions for 28 d. After the initial set of the grouting material was completed in 5 d, the reinforcement cages of the piers were started. Rebar with a diameter of 28 mm and a design tensile strength of 400 MPa was used as the main reinforcement of the pier. The last step of the construction was a coarse aggregate concrete that was poured into the pit (Fig. 3g). The compressive strength of concrete under 28 d of standard curing conditions was 30 MPa. While the foundations were cured, the test components were fabricated and transported, including concrete blocks (Fig. 3h), steel plates, and steel beams. After all the conditions met the requirements, the test system was built, including the installation of steel beams, commissioning of instruments, and connector welding (Fig. 3i).

2.2 Loading system and test program

The loading system and testing devices included one loading beam (H-beam), four main beams (H-beams), a hydraulic loading system, a supporting system, dial gauges, and monitoring devices. A total of

Table 1 Dimension information of test foundations

Foundation	L_p (m)	L_a (m)	d_1 (m)	d_2 (m)	d_a (mm)	d_b (mm)	Number of anchors
A-1	3	1	1	1.5	120	40	4
A-2	3	2	1	1.5	120	40	4
A-3	3	3	1	1.5	120	40	4

Fig. 3 Overview of construction, including: (a) geological survey and site selection; (b) sampling and testing of soil and rock; (c) excavating the belled pier; (d) drilling of boreholes; (e) preparation of reinforcement and sensors; (f) positioning and installation of steel bars and sensors; (g) foundation pouring; (h) fabrication of test components; (i) construction of the test system

six dial gauges were used to measure the displacement of the foundation and ground surface in each loading stage and were arranged in two groups on each anchored pier foundation. Two of the dial gauges were symmetrically arranged at the top of the foundation, and the others were arranged around the foundation, with a spacing of 1.5 m from the center point of the top surface of the foundation. Fig. 4 presents a schematic profile of the test setup. The steel bars in the foundation were positioned 2.5 m above the top surface of the foundation, and each bar was welded with the steel connector on both sides.

Strain gauges and earth pressure cells were embedded in the foundations. Strain gauges were placed at the joints between the anchors and the belled piers so that the loads of the anchor groups could be obtained.

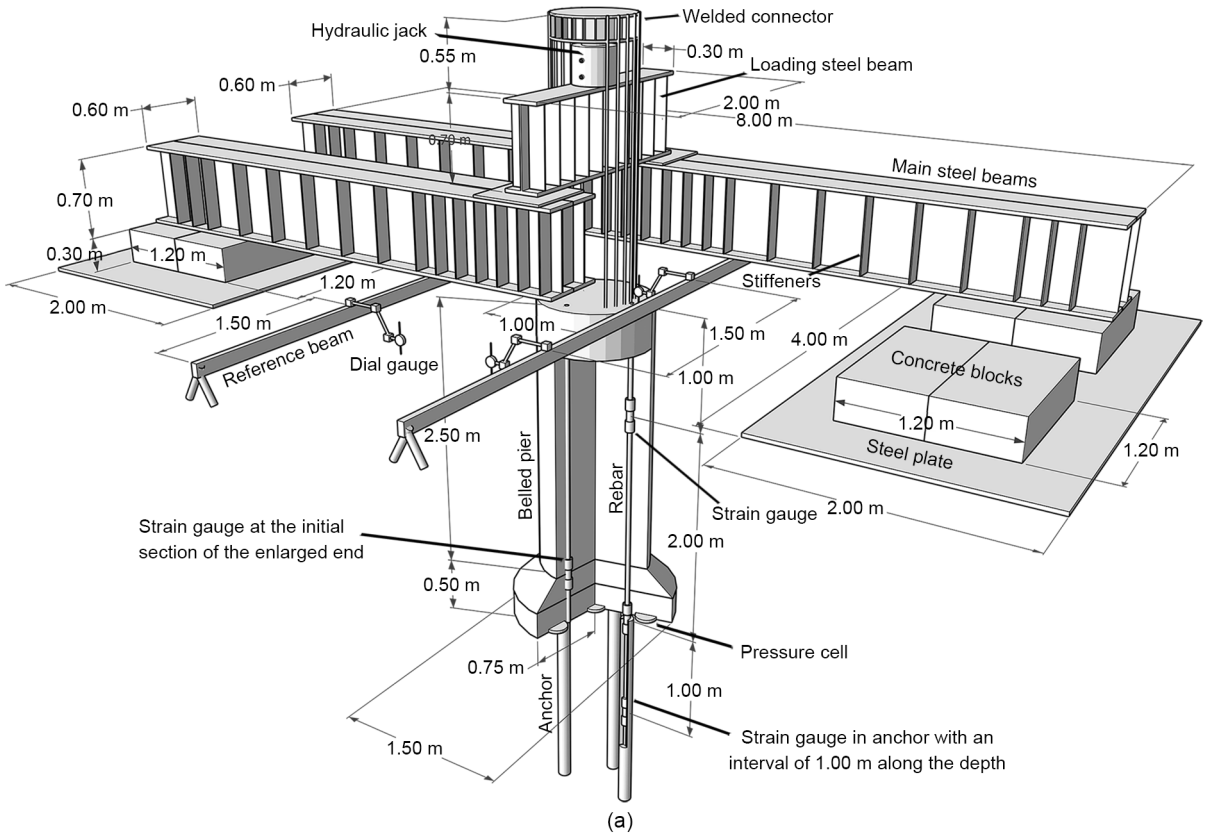

Fig. 4 Field tests: (a) schematic profile of the test setup; (b) site photo

At intervals of 1 m, the strain gauges in each anchor were arranged on the steel bar. Another group of strain gauges was arranged 1 m below the top of the foundation and at the point where the straight section met the enlarged base. Each of the two groups comprised four strain gauges, which were installed symmetrically on the same section. Strain gauges were connected to steel bars through sleeves of matching sizes to ensure coaxiality and reliability. Five earth pressure cells were evenly and horizontally distributed on the pre-grooved rock surface under each belled pier. Each earth pressure cell was wrapped with geotextile and was padded with sand on the top and bottom to avoid the influence of concrete solidification and to ensure the uniform and vertical transmission of pressure. Both the strain gauge and the earth pressure cell were vibrating-wire sensors.

According to ASTM D3689/D3689M-07(2013)e1 (ASTM, 2013), the slowly maintained load method was used for all of the uplift tests. During the uplift

tests of each foundation, the load was gradually increased by 10% of the expected ultimate load of each foundation. Every load stage was maintained until the two consecutive displacements within each hour were less than 0.1 mm; then the next stage was conducted. The test continued after the pullout displacement of each stage was stabilized, while the loading stopped until the uplift rate exceeded the above-mentioned standard.

2.3 Geology conditions

It can be estimated from the continuous core samples (Fig. 3b) and foundation construction that the thickness of the soil layer was about 2.5 m and was followed by weathered rock. On the basis of the categorization standards for rock and soil (ASTM D2487-17e1 and D6032/D6032M-17) (ASTM, 2017a, 2017b), laboratory tests were conducted. The range of the parameters was established by testing on the rock and soil using sieving analysis. Fig. 5a shows the particle gradation of the soil within the buried depth of the belled pile, which can be classified as SP (poorly graded sand with gravel) according to ASTM D2487-17e1. The rock samples completed point-load and uniaxial compression testing to gauge their strength. Examples of test samples are shown in Fig. 5b. The rock classes are listed in Section S1 of the electronic supplementary materials (ESM) according to rock mass classification standard ASTM D5878-19 (ASTM, 2019). According to the rock mass rating system (RMR), the ratings of the cores at foundations A-1, A-2, and A-3 are 35, 36, and 25, respectively, all of which are classified as Class IV poor rocks.

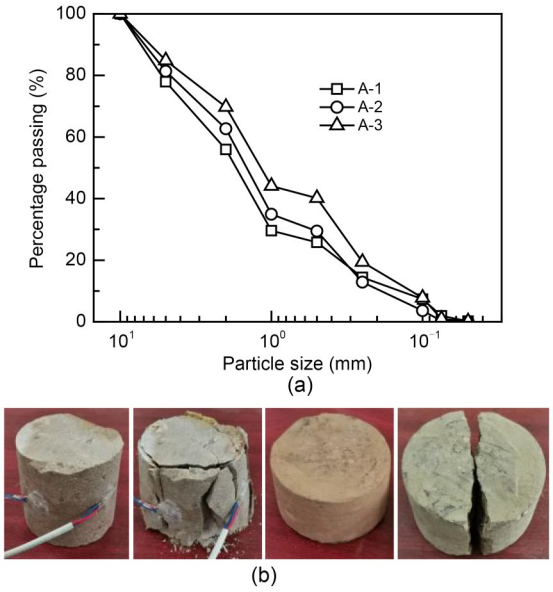

Fig. 5 Laboratory tests of soil and rock: (a) typical particle gradation of the soil; (b) in-situ core samples

The deformation modulus of the soil can be estimated according to a chart of the flat dilatometer test (DMT) proposed by Marchetti and Crapps (1981). The details of their estimation method are presented in Section S2 of the ESM. The geological parameters of each test point are shown in Table 2.

3 Analysis of the experimental results

3.1 Processing of the experimental results

The measured uplift *P-s* curves of all foundations are shown in Fig. 6. The value of the loading in the test results was converted from the pressure of the jack. s_f is the displacement of the anchored pier, which is the average of the measured readings of the two dial gauges at the top of the foundation. The *P-s* curves of the anchored pier foundation, as well as those of the belled piers and anchor groups, are shown in Fig. 6. s_p is the displacement of the pier, which is consistent with the displacement of the anchored pier. s_a is the displacement of the anchor group obtained by removing the elastic deformation of the pier from the s_f. The displacement conversion process of the anchor group is expressed as

$$s_{ai}=s_{fi}-L_p\cdot\frac{P_{fi}}{A_pE_c}, \tag{1}$$

where s_{ai} and s_{fi} are the uplift displacements of the anchor group and anchored pier foundation at the *i*th loading stage, respectively; L_p is the buried depth of the belled pier (which is 3 m); P_{fi} is the loading value of stage *i*; A_p is the cross-sectional area of the pier

Table 2 Geological parameters

Item	Depth, h_d (m)	Unit weight, γ (kN/m^3)	Poisson's ratio, v	Deformation modulus, E (MPa)
Soil layer (gravel sand)	2.5	22	0.25	83–188
Rock layer (strongly weathered tuff)	>2.5	23	0.30	486–1115

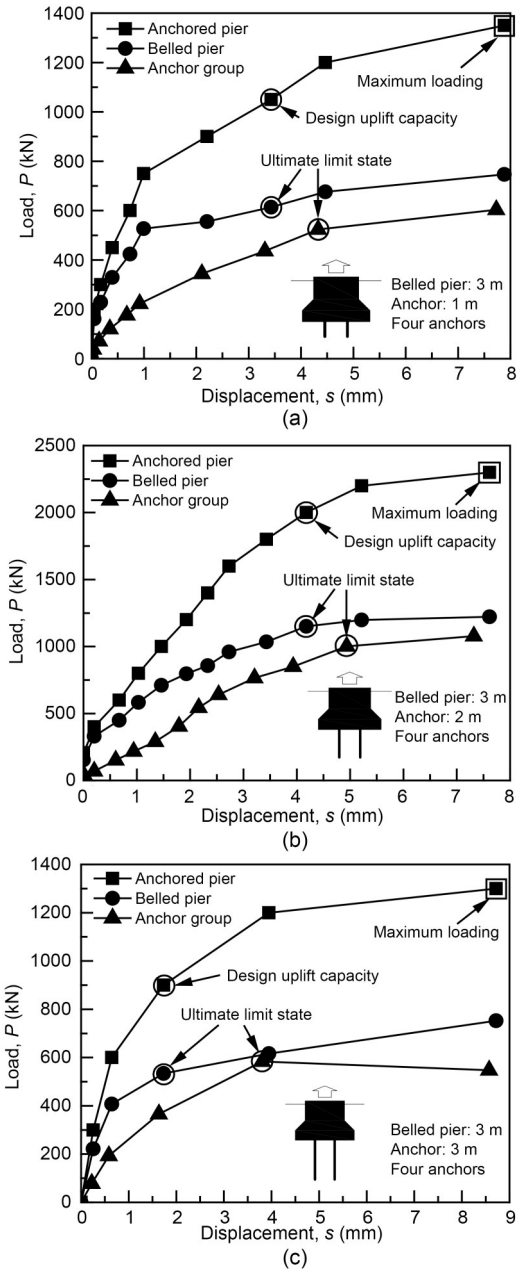

Fig. 6 Load–displacement curves of the anchored pier foundations: (a) A-1; (b) A-2; (c) A-3

column (which is 0.785 m^2); E_c is the tensile modulus of elasticity of concrete. The ultimate uplift capacity (UUC) and the ULS of the anchored pier are determined by the tangential intersection method (Hirany and Kulhawy, 1988) of the *P-s* curve, with the details shown in Section S3 of the ESM.

The total force measured by four strain gauges placed at the intersections of the anchors and the belled pier of each foundation was translated into the load of the anchor group (P_a). By deducting P_a from the pullout load of the anchored pier (P_f), the load of the belled pier (P_p) was determined.

The uplift capacity may be represented as

$$P_f = k_1 P_p + k_2 P_a, \tag{2}$$

where k_1 and k_2 are the UMCs of the pier and the anchor group, respectively.

According to the definition of the serviceability limit state (SLS), neither the pier nor the anchor group reaches the ULS until the anchored pier reaches the SLS. The first component (pier or anchor group) to reach the ULS is the controlling factor for the SLS of the anchored pier foundation. Based on the analysis of the *P-s* curves and the determination of the ULS, it can be found that the pier is the first to reach its ULS. Table 3 shows the test results and corresponding k_1 and k_2 values of the hybrid foundation at its design uplift capacity (DUC). It can be seen that, when the DUC of the hybrid foundation is reached, k_1 equals 1, that is, the belled pier reaches its ULS. The k_2 value is less than 1, which means that the anchor group has not fully reached its UUC. The test data show that A-2 had a better uplift capacity than A-3 for the belled pier and anchor group. Differences in geology and construction caused this significant difference. Geologically, the uniaxial compressive strength of the cores from A-2 (12.17 MPa) is much greater than that of A-3 (1.37 MPa). Considering the condition of discontinuities and quality of the rock, the RMR of A-2 rock (36) is also higher than that of A-3 rock (25), as shown in Section S1. This results in the uplift capacity of foundation A-2 being greater than that of foundation A-3. In terms of construction, there were more stones in the burial depth of the A-2 pier,

Table 3 Pullout test results for all foundations

Foundation	UUC (kN)			UMC		DUC of the anchored pier (kN)
	P_{fu}	P_{pu}	P_{au}	k_1	k_2	
A-1	1200.0	614.0	524.0	1.00	0.83	1050.0
A-2	2200.0	1150.0	1001.6	1.00	0.85	2000.0
A-3	1200.0	534.1	583.6	1.00	0.63	900.0

and the vacancies created by falling stones during manual excavation increased the concavity of the sidewalls. This can be confirmed in Fig. 7. The friction and bite force between the foundation sidewall and the geotechnical body are the components that constitute the uplift capacity of the anchored pier. Thus, the pier of A-2 with rougher sidewalls had a higher uplift capacity, as shown in Table 3.

Fig. 7 Comparison of sidewalls and surrounding soil: (a) A-2; (b) A-3

3.2 Load distribution of pier and anchor

The strain gauge readings were calculated and processed to obtain the forces in each section of the foundation. The following equation gives the calculation of the forces:

$$T_{ij}=\sigma_{ij}A_{\mathrm{s}}+\sigma_{ij}(A_{\mathrm{c}}-A_{\mathrm{s}})\cdot\frac{E_{\mathrm{c}}}{E_{\mathrm{b}}}, \tag{3}$$

where subscripts i and j represent the loading stage and section, respectively; T_{ij} and σ_{ij} are the force and stress at the loading stage and section, respectively; A_{c} is the cross-sectional area of the foundation in addition to the reinforcement, which is 0.785 m^2; A_{s} is the sum of the sectional areas of all reinforcement, which is 0.015 m^2; E_{c} and E_{b} are the elasticity moduli of concrete and reinforcement, respectively. The values of 27.5 and 200.0 GPa for E_{c} and E_{b}, respectively, were obtained from the sample tests.

The load distribution of the foundation is shown in Fig. 8. The resistance curves for the depths of the various stages reveal that the resistance of the increased bottom, the side friction of the pier column, and the anchoring force of the anchor group made up the three components of the uplift capacity of the

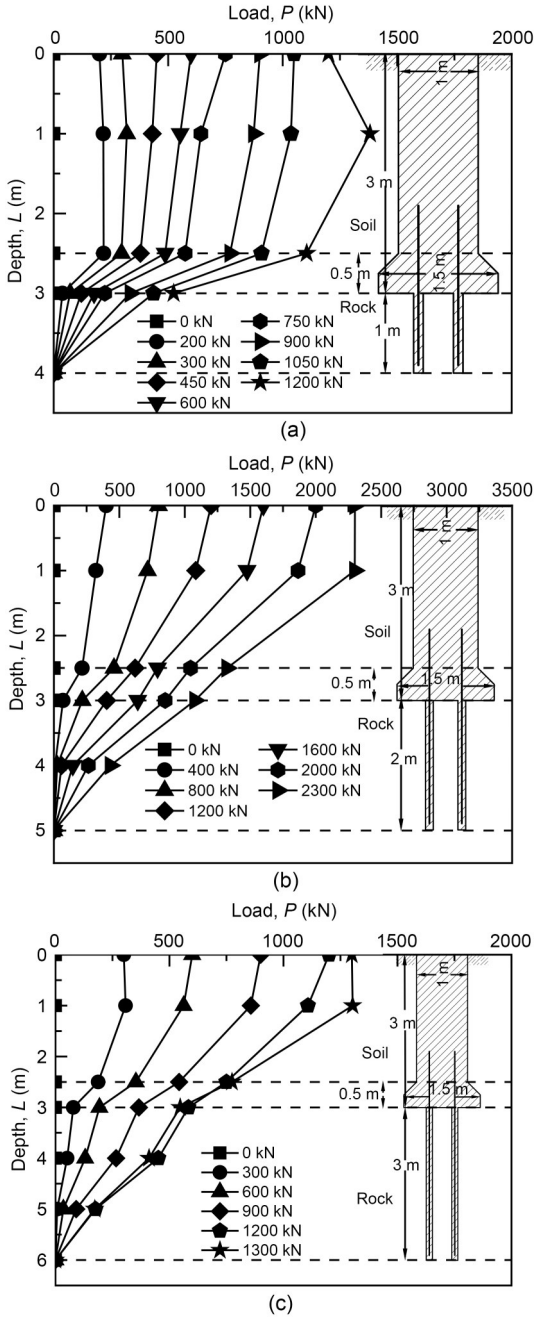

Fig. 8 Axial force distribution: (a) A-1; (b) A-2; (c) A-3

foundation. As the load increased, the pullout resistance provided by each part increased. In the final stage curve in Fig. 9, the force of the pier column was greater than the load placed on the foundation. This indicates that the stresses in the foundation sections derived from the reinforcement stresses exceed the actual values. The concrete and the reinforcement appeared to be incompatible in terms of deformation, i.e., cracks appeared.

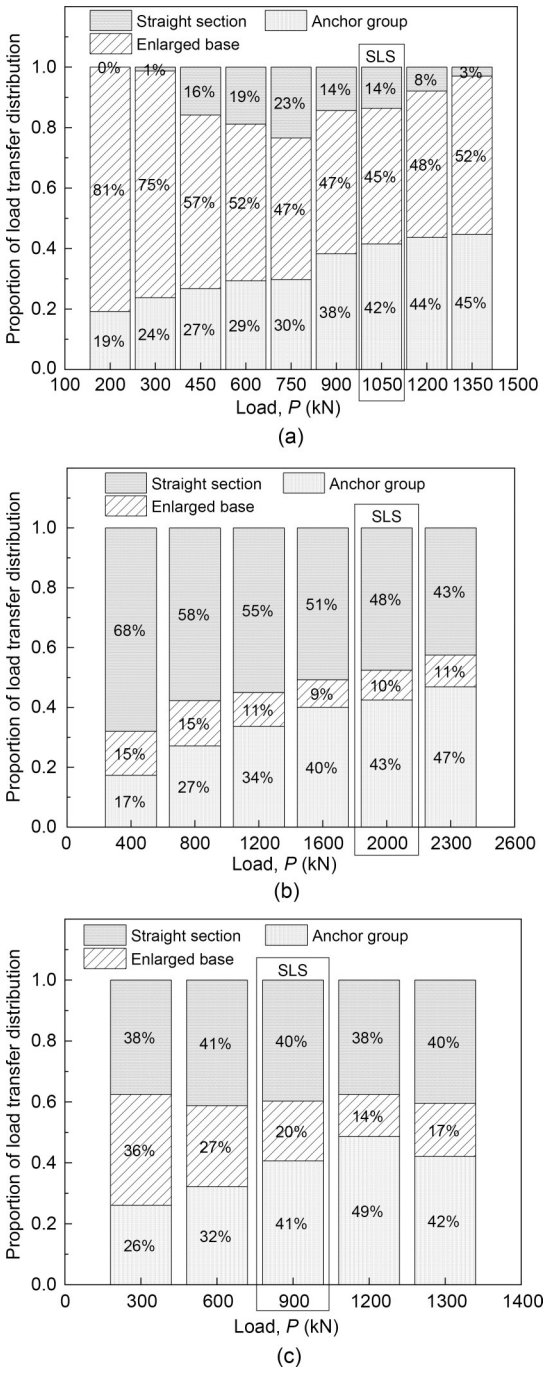

Fig. 9 Load distribution: (a) A-1; (b) A-2; (c) A-3

Fig. 9 shows the load distribution. It can be seen that before reaching the DUC, the proportion of the load of the pier under each stage decreased step-wise while the proportion of the anchor group increased. For the pier, as the load developed previous to the ULS, the percentage of the load carried by the larger bottom steadily dropped. The uplift capacity was determined by the total shear capacity of the surrounding soil, and the weight of the soil and foundation. Furthermore, the proportion of the anchor group gradually increased from about 20%, in the initial stages, to about 40% in the final stages. The load distribution ratio of the anchor group tended to stabilize or decline (A-3) after the ULS was reached.

The above study shows that for anchored piers with similar geometry as the ones in this test, belled piers and anchor groups determine the SLS and ULS of the anchored piers, respectively. The determination of the DUC at the SLS is critical to the design of the foundation (Phoon, 2006; Tang and Phoon, 2018).

3.3 Failure mechanism of belled pier

The surface displacement changed significantly after the anchored pier foundation reached the ULS, and cracks appeared around the foundation, as shown in Fig. 10a. The cracks spread around in a roughly emissive shape, indicating an uplift deformation of the surrounding soil. Fig. 11a shows the displacement results of the top surface of the anchored pier foundation and the ground surface 1.5 m from the center of the foundation. Extracting the displacement measurement results of the A-1 foundation at 1350 kN, the contour diagram, as shown in Fig. 11b, can be drawn. The contour diagram gives the variation from the uplift displacement of 0 mm at a position 3.5 m from the center of the foundation to the uplift displacement of 8 mm at the top side edge of the foundation. From the test results regarding the uplift displacement, it can be seen that the displacement of the ground surface 1.5 m from the center of the foundation is much smaller than that for the foundation at the corresponding loading stage.

3.4 Failure mechanism of anchor group

Fig. 12 illustrates the uplift loads (measured by strain gauges) of the pier and anchor group at each stage compared to the forces at the bottom of the pier measured by the pressure cells. The uplift loads of the pier and anchor group correspond to the left *y*-axis, and the bottom force corresponds to the right *y*-axis. The bottom force was obtained by multiplying the average pressure measured by the pressure cells by the bottom area of the pier. As the uplift load increased, the bottom of the pier was gradually pulled away from the lower rock mass, and the pressure decreased. At the maximum loading, the corresponding changes

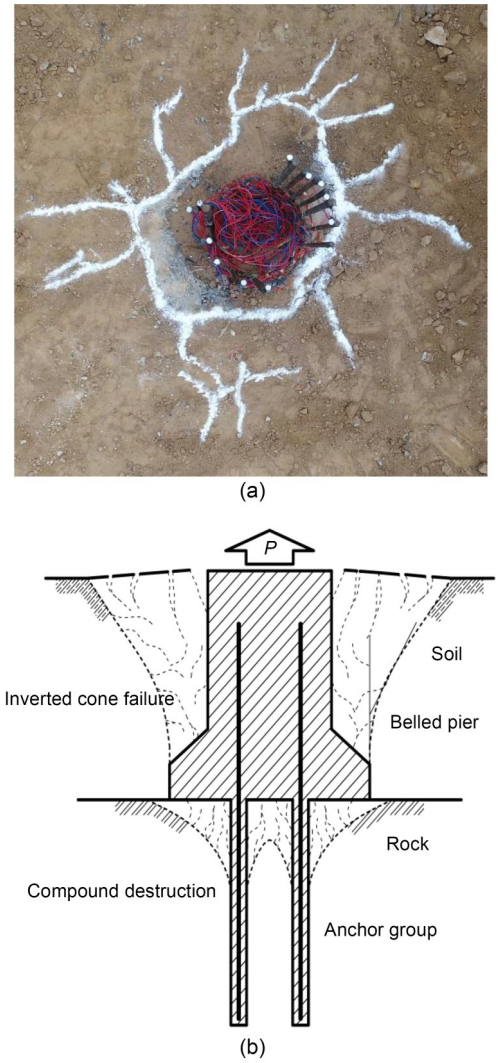

Fig. 10 Failure mode: (a) surface crack map of foundation A-1; (b) schematic of the failure mode

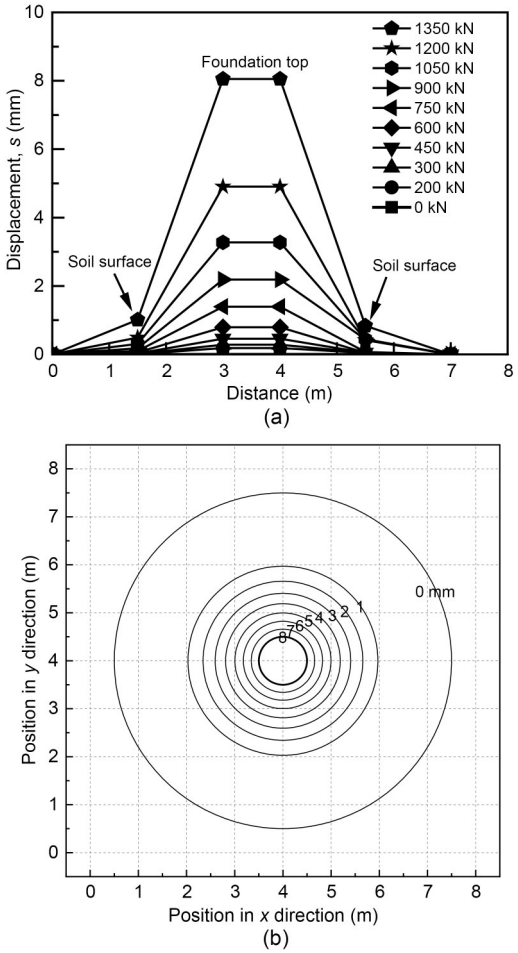

Fig. 11 Measured displacements of the foundation and soil surface (A-1 as an example): (a) foundation and ground displacement under various loads; (b) contour diagram of soil surface around A-1 at 1350 kN

in the bottom force of A-1, A-2, and A-3 are −12.8, −39.4, and −4.2 kN, respectively. However, the force at any stage was much smaller than the weight of the belled pier (66.55 kN), which showed that the underlying layer was still attached to the bottom of the belled pier.

Further, the mobilization of the failure surface and the failure mode of the anchored pier can be considered. According to the classification proposed by Pacheco et al. (2008), the failure mode of the piers in this study belongs to the shallow mode. At the early stage of uplift, the friction of the pier-soil surface was gradually exerted with the increase of load. A relative slip of the sidewall and soil appeared and the failure surface developed downward. With the transfer of load to the bottom of the pier, the belled bottom began to squeeze the upper soil (soil was sheared), and the anchoring force of the anchor came into play, at which time the failure surface extended to the belled bottom. The pier was the first to reach the ULS, and the surrounding soil experienced overall shear damage, with the failure surface penetrating from the bottom of the pier to the ground (inverted cone failure) (Das, 2017). At this time, the failure surface also appeared at the interface between the anchor and the rock and developed. The rock around the upper part of the anchor was subjected to shear and tensile forces resulting in fissures. At the ULS of the anchor, the rock around the initial section of the anchor underwent overall shear damage, forming an inverted cone pullout body, as can be surmised from the previous analysis of the pressure cell results. Referring to the study by Serrano

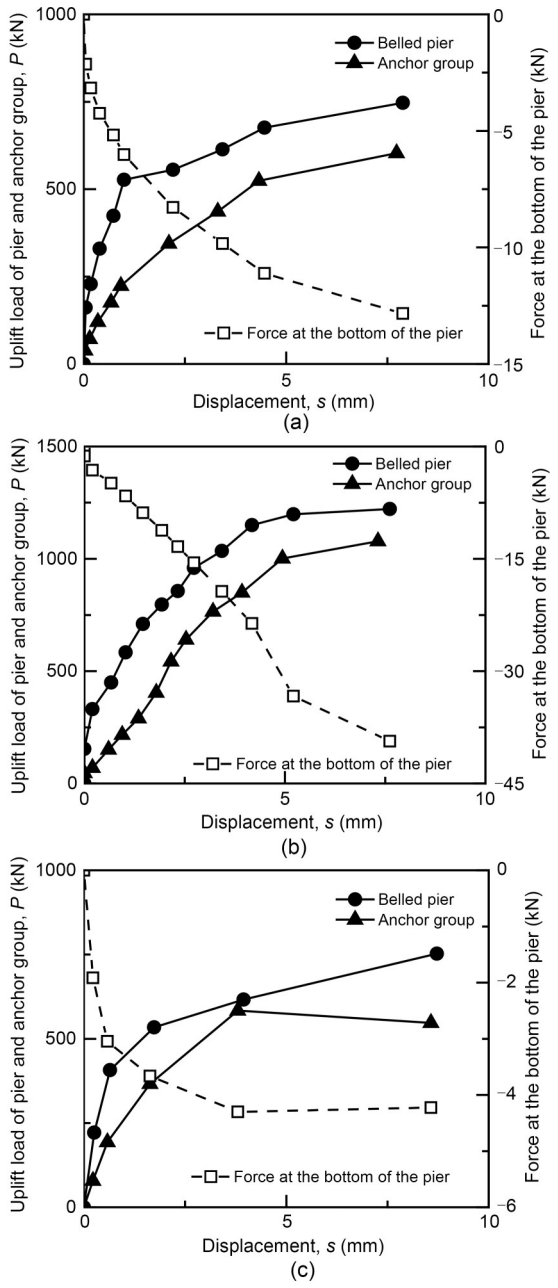

Fig. 12 Comparison of the uplift loads of the pier and anchor group at each stage with the force at the bottom of the pier as measured by the pressure cells: (a) A-1; (b) A-2; (c) A-3

and Olalla (1999), compound destruction was the failure mode of the anchor groups in this test. The failure surface in the lower part of the anchor was at the anchor–rock interface, while in the upper part of the anchor, it extended outward into the rock mass. Fig. 10b is a schematic diagram of the failure mode of the anchored pier.

4 Calculation theory of monotonic uplift capacity

The calculation method can be expanded and supplemented based on existing design codes (IEEE, 2001; BSI, 2013) and studies on piers (Das, 2017) and anchors (Serrano and Olalla, 1999), in terms of DUC calculations, design processes, and construction requirements. To the best of our knowledge, the combination of these two foundations (anchored pier foundations) has not been specified in any previous studies or standards. The special parameters, UMCs, which reflect the load distribution of this foundation, need to be determined in the uplift capacity calculation and the design process. Although it was observed from the three tests that the anchor groups reached the ULS before the piers (k_1<1, k_2=1), it did not rule out that the pier reached the ULS before the anchor group. Therefore, considering the applicability of the UMC calculation method, one of k_1 and k_2 can be assumed to be equal to 1 in the derivation, and then the equation of the other can be given (as discussed below).

4.1 Calculation method for the UMC

Assume the case where k_1=1 to solve for k_2 as an example for analysis. First, the load-transfer equation of the pier is as follows, following research on the uplift capability of the pier (Chow, 1986):

$$\frac{\partial}{\partial r}(r\tau)+r\frac{\partial \sigma_z}{\partial z}=0, \tag{4}$$

where r is the radius of the foundation, σ_z is the total stress in the vertical direction, and τ is the shear stress on the side of the foundation.

The concept of influencing radius r_m proposed by Randolph (1978) is crucial for the calculation of the uplift capacity. The following equation can be used to determine the initial uplift stiffness of the belled pier (K_p) with the introduction of r_m:

$$K_p=\frac{P_p}{s}=\left[\frac{4(r_0+r_d)}{r_0(1-v_s)}+\frac{2\pi L_p}{\xi r_0}\right]\cdot Gr_0, \tag{5}$$

where G is the shear modulus of soil; $\xi=\ln(r_m/r_0)$ is the Randolph influencing radius coefficient; $r_m=2.5\rho L_p(1-v_s)$ is the Randolph influencing radius; v_s is Poisson's ratio of the soil; $\rho=G_h/G_n$ represents the

ratio of the soil shear modulus at the middle and bottom of the pier depth. For shallow foundations, ρ is equal to 1. r_0 and r_d are the radii of the pier column and the enlarged bottom, respectively.

The above calculations can only obtain the uplift *P-s* relationship of the belled pier in the elastic state. In fact, the uplift *P-s* curves of foundations are typically very nonlinear. A normalized hyperbolic model proposed by Chin (1970) can be used to fit these curves. Some pile tests were conducted by Castelli et al. (1991) to verify the validity of this theory with the introduction of initial tangent stiffness (i.e., initial uplift stiffness mentioned above) and hyperbolic fitting coefficient R_f. The uplift load and displacement have a nonlinear connection that may be represented as:

$$P=\frac{s}{a+b\cdot s}, \tag{6}$$

where $a=1/K$ is the initial stiffness coefficient; K is the initial uplift stiffness; $b=R_f/P_u$ is the bearing capacity coefficient; P_u represents the UUC of the foundation; the hyperbolic fitting coefficient, R_f, is a value that spans from 0.7 to 1.0. The value of R_f is related to the form of the *P-s* curve, which varies from 0.7 to 1.0 corresponding to a slowly varying curve moving to a steeply varying curve (Kulhawy and Hirany, 1989; Phoon, 2006; Qian et al., 2014). For rock foundations and pier foundations in soil, the values can be taken as 0.7 and 1.0, respectively.

Eq. (6) is also suitable for fitting the *P-s* curve of the anchor. Therefore, to calculate the pullout load P_a of the anchor, the initial uplift stiffness of anchor (K_a) and the UUC need to be determined.

According to the study on the pullout deformation and stiffness of grouted rock anchors made by Cai et al. (2004), the initial uplift stiffness of anchors is calculated as

$$K_a=\frac{P_a}{s}=\pi r_b^2 E_b \beta \tanh(\beta L_a), \tag{7}$$

where $\beta=\sqrt{2k/(r_b E_b)}$ is the initial stiffness factor; the radii of the anchor bar and hole, respectively, are r_b and r_g; the elasticity moduli of the anchor bar and grouting material, respectively, are E_b and E_g; $k=G_g G_r/\left[G_r r_b \ln\left(r_g/r_b\right)+G_g r_b \ln\left(R/r_g\right)\right]$ is the elastic shear stiffness between the anchor bar and rock; $R=10E_b r_b/\left[(E_g+E_r)/2\right]$ is the influencing radius of uplift deformation; E_r is the deformation modulus of the rock; G_g is the shear modulus of the grouting material; G_r is the shear modulus of the rock; L_a is the length of the anchor shaft.

Based on the above analysis, the expression for k_2 can be obtained, as follows:

$$\begin{aligned}k_2&=\frac{P_a}{P_{au}}=\frac{s/(a_2+b_2 s)}{P_{au}}=\frac{a_1 P_p}{a_2 P_{au}+(a_1 b_2-a_2 b_1)P_p P_{au}}\\&=\frac{K_a P_p P_{pu}}{R_{f2}K_a P_p P_{pu}+\left(P_{pu}-R_{f1}P_p\right)K_p P_{au}},\end{aligned} \tag{8}$$

where a_1 and a_2 are the initial uplift coefficients of the pier and anchor, respectively; b_1 and b_2 are the bearing capacity coefficients of the pier and anchor, respectively; R_{f1} and R_{f2} are the hyperbolic fitting coefficients of the pier and anchor, respectively. In the service-limit state of the anchored pier, $P_p=P_{pu}$, so k_2 can be calculated as:

$$k_2=\frac{K_a P_{pu}}{(1-R_{f1})K_p P_{au}+R_{f2}K_a P_{pu}}. \tag{9}$$

Similarly, the case when $k_2=1$ is analyzed, and the expression for k_1 is obtained, as follows:

$$\begin{aligned}k_1&=\frac{P_p}{P_{pu}}=\frac{s/(a_1+b_1 s)}{P_{pu}}=\frac{a_2 P_a}{a_1 P_{pu}+(a_2 b_1-a_1 b_2)P_a P_{pu}}\\&=\frac{K_p P_a P_{au}}{R_{f1}K_p P_a P_{au}+(P_{au}-R_{f2}P_a)K_a P_{pu}},\end{aligned} \tag{10}$$

where, in the service-limit state of the anchored pier, $P_a=P_{au}$, so k_1 can be calculated as:

$$k_1=\frac{K_p P_{au}}{(1-R_{f2})K_a P_{pu}+R_{f1}K_p P_{au}}. \tag{11}$$

Eq. (9) or Eq. (11) can be used to calculate the UMC, and the results can then be entered into Eq. (2) to determine the uplift capacity of the anchored pier. The calculation procedure of the UMC is shown in Section S4 of the ESM, along with the UMC of A-1 as a case.

4.2 Calculation process of monotonic uplift capacity

Fig. 13 shows the fitting results of the analytical solution of the hyperbolic model based on Eq. (6) and

the experimental data of A-1. The deformation moduli of the soil and the rock mass are taken as 174 and 1034 MPa, respectively, based on the estimation method. The dimensional parameters are shown in Table 1. According to the characteristics of the *P-s* curves, the hyperbolic fitting coefficients corresponding to the pier and the anchor group can be taken as R_{f1}=0.7 and R_{f2}= 1.0, respectively. The hyperbolic model matches well with the trend of the measured *P-s* curve. It can be noted that in the initial pullout phase of the anchor group, the measurement results deviate from the hyperbolic model. The measured initial uplift stiffness K_a (slope) of the anchor group is lower than that of the hyperbolic model. The reason for this could be twofold. On the one hand, the fractures and weak layers in the rock mass make the K_a lower than that calculated from the core samples. On the other hand, there may be a small relative sliding at the interface between the concrete and the rock, which reduces the K_a.

The three anchored piers of this test and the foundations (anchored piers CF-A and CF-B, and combination foundation GTC2+AG8) reported in other studies (Ismael et al., 1979; Cheng et al., 2012; Qian et al., 2015) were used as examples for the verification of the calculation method proposed above, and the results are shown in Table 4. Details of other foundations are shown in Section S5 of the ESM. The theoretical method proposed to determine the UMC and the uplift capacity can be used to calculate the DUC of the anchored pier. Except for A-3, the difference between the physical test and the calculation approach for P_f for each of the foundations is within 10%. As mentioned earlier, differences in geology and construction (Fig. 7) led to anomalies in the A-3 results, thus increasing the difference between the measured and theoretical calculations of P_f. It is important to note that k_2 does not indicate the individual uplift properties of anchors. Its significance is reflected in the process of calculating the uplift capacity of the anchored pier.

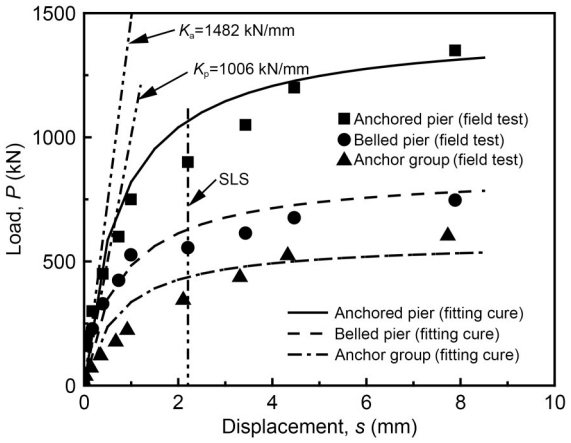

Fig. 13 *P-s* curves of the foundation A-1 as fitted by hyperbolic models

5 Conclusions

Three in-situ monotonic uplift tests performed on the anchored pier foundations have been described in this paper. Through analysis and fitting of the test results, the uplift behavior characteristics and the UMC calculation methods for the anchored pier foundations are given and the conclusions shown below can be reached for the structural configurations and geological conditions considered.

1. The uplift capacity of anchored pier is mainly provided by two parts: the belled pier and the anchor group. The uplift capacity of the former is composed of the side friction and the shear effect of the undisturbed soil on the enlarged bottom, while the latter is the anchorage force on the rock.

2. The first part that reached the UUC is the control factor for the SLS of the anchored pier. Due to the load distribution, the uplift capacity of the foundation

Table 4 Comparison of the experimental and calculated results (Ismael et al., 1979; Cheng et al., 2012; Qian et al., 2015)

Foundation	P_{pu} (kN)	P_{au} (kN)	Test			Calculation			Difference in P_f
			k_1	k_2	P_f (kN)	k_1	k_2	P_f (kN)	
A-1	614.0	524.0	1	0.83	1050.0	1	0.85	1059.4	0.9%
A-2	1150.0	1001.6	1	0.85	2000.0	1	0.85	2001.4	0.1%
A-3	534.1	583.6	1	0.63	900.0	1	0.87	1041.8	15.8%
CF-A	1080.0	900.0	1	1.00	2000.0	1	1.00	1980.0	1.0%
CF-B	1200.0	1080.0	1	0.97	2250.0	1	0.78	2042.0	9.2%
GTC2+AG8	1288.0	1340.0	1	0.92	2521.0	1	0.96	2574.0	2.1%

can be calculated by the UMCs and the uplift capacity of each part.

3. A combination of the failure mechanisms of the belled pier and the anchor group characterizes the failure mode of the anchored pier at the uplift ULS.

4. The anchored pier foundation is an independent foundation that can be flexibly adjusted according to geological conditions. Based on the theory of belled piers and anchors, the anchored pier foundation design should include a load distribution analysis to determine the SLS and the DUC.

5. The UMCs can be effectively obtained by substituting the survey results (geology and dimensions) into the theoretical calculation method proposed in this paper. They provide a basis for the calculation of uplift capacity and the design of the anchored pier foundation.

Acknowledgments

This work is supported by the National Natural Science Foundation of China (No. U2006225) and the European Union's Horizon 2020 Marie Skłodowska-Curie Research and Innovation Staff Exchange Programme (No. 778360).

Author contributions

Yizhou SUN designed the research and wrote the first draft of the manuscript. Honglei SUN helped to organize the manuscript. Chong TANG, Yuanqiang CAI, and Feng PAN revised and edited the final version.

Conflict of interest

Yizhou SUN, Honglei SUN, Chong TANG, Yuanqiang CAI, and Feng PAN declare that they have no conflict of interest.

References

ASTM (American Society for Testing and Materials), 2013. Standard Test Methods for Deep Foundations Under Static Axial Tensile Load, ASTM D3689/D3689M-07(2013)e1. ASTM, USA. https://doi.org/10.1520/D3689_D3689M-07R13E01

ASTM (American Society for Testing and Materials), 2017a. Standard Practice for Classification of Soils for Engineering Purposes (Unified Soil Classification System), ASTM D2487-17e1. ASTM, USA. https://doi.org/10.1520/D2487-17E01

ASTM (American Society for Testing and Materials), 2017b. Standard Test Method for Determining Rock Quality Designation (RQD) of Rock Core, ASTM D6032/D6032M-17. ASTM, USA. https://doi.org/10.1520/D6032_D6032M-17

ASTM (American Society for Testing and Materials), 2019. Standard Guides for Using Rock-Mass Classification Systems for Engineering Purposes, ASTM D5878-19. ASTM, USA. https://doi.org/10.1520/D5878-19

BSI (British Standards Institution), 2013. Execution of Special Geotechnical Works–Ground Anchors, BS EN 1537: 2013. BSI, UK.

Cai Y, Esaki T, Jiang YJ, 2004. An analytical model to predict axial load in grouted rock bolt for soft rock tunnelling. *Tunnelling and Underground Space Technology*, 19(6): 607-618. https://doi.org/10.1016/j.tust.2004.02.129

Castelli F, Maugeri M, Motta E, 1991. Analisi non lineare del cedimento di un Palo Singolo. Rivista Italiana di Geotecnica, p.115-135 (in Italian).

Cheng YF, Lu XL, Ding SJ, et al., 2012. Experimental and computational research on the uplift of composite foundation of belled pier and rock anchor in transmission line engineering. *Electric Power Construction*, 33(3):6-10 (in Chinese). https://doi.org/10.3969/j.issn.1000-7229.2012.03.002

Chin FK, 1970. Estimation of the ultimate load of piles from tests not carried to failure. Proceedings of the 2nd Southeast Asian Conference on Soil Engineering, p.81-92.

Chow YK, 1986. Analysis of vertically loaded pile groups. *International Journal for Numerical and Analytical Methods in Geomechanics*, 10(1):59-72. https://doi.org/10.1002/nag.1610100105

Das BM, 2017. Shallow Foundations: Bearing Capacity and Settlement. 3rd Edition. CRC Press, Boca Raton, USA. https://doi.org/10.1201/9781315163871

Fabris C, Schweiger HF, Pulko B, et al., 2021. Numerical simulation of a ground anchor pullout test monitored with fiber optic sensors. *Journal of Geotechnical and Geoenvironmental Engineering*, 147(2):04020163. https://doi.org/10.1061/(ASCE)GT.1943-5606.0002442

Harris DE, Madabhushi GSP, 2015. Uplift capacity of an underreamed pile foundation. *Proceedings of the Institution of Civil Engineers-Geotechnical Engineering*, 168(6):526-538. https://doi.org/10.1680/jgeen.14.00154

Hirany A, Kulhawy FH, 1988. Conduct and Interpretation of Load Tests on Drilled Shaft Foundations: Volume 1, Detailed Guidelines. Technical Report No. EPRI-EL-5915-Vol.1, Electric Power Research Institute, Palo Alto, USA.

Honda T, Hirai Y, Sato E, 2011. Uplift capacity of belled and multi-belled piles in dense sand. *Soils and Foundations*, 51(3):483-496. https://doi.org/10.3208/sandf.51.483

IEEE (Institute of Electrical and Electronics Engineers), 2001. IEEE Guide for Transmission Structure Foundation Design and Testing, IEEE Std 691-2001. IEEE, USA. https://doi.org/10.1109/IEEESTD.2001.93372

Ismael NF, Radhakrishna HS, Klym TW, 1979. Uplift capacity of rock anchor groups. *IEEE Transactions on Power Apparatus and Systems*, 98(5):1653-1658. https://doi.org/10.1109/TPAS.1979.319483

Jia YZ, Wang MQ, Zhang J, et al., 2014. The numerical

simulation analysis of transmission lines new composite type foundation. *Applied Mechanics and Materials*, 459: 641-645. https://doi.org/10.4028/www.scientific.net/amm.459.641

Kim HK, Cho NJ, 2012. A design method to incur ductile failure of rock anchors subjected to tensile loads. *Electronic Journal of Geotechnical Engineering*, 17:2737-2746.

Kulhawy FH, 2015. Discussion of "instrumented static load test on rock-socketed micropile" by Hoyoung Seo, Monica Prezzi, and Rodrigo Salgado. *Journal of Geotechnical and Geoenvironmental Engineering*, 141(6):07015002. https://doi.org/10.1061/(ASCE)GT.1943-5606.0001263

Kulhawy FH, Hirany A, 1989. Interpretation of load tests on drilled shafts—part 2: axial uplift. Foundation Engineering: Current Principles and Practices, p.1150-1159.

Li LC, Zheng MY, Liu X, et al., 2022. Numerical analysis of the cyclic loading behavior of monopile and hybrid pile foundation. *Computers and Geotechnics*, 144:104635. https://doi.org/10.1016/j.compgeo.2022.104635

Ma SQ, Nemcik J, Aziz N, et al., 2016. Numerical modeling of fully grouted rockbolts reaching free-end slip. *International Journal of Geomechanics*, 16(1):04015020. https://doi.org/10.1061/(ASCE)GM.1943-5622.0000484

Ma TH, Li CJ, Lu ZM, et al., 2015. Rainfall intensity–duration thresholds for the initiation of landslides in Zhejiang Province, China. *Geomorphology*, 245:193-206. https://doi.org/10.1016/j.geomorph.2015.05.016

Marchetti S, Crapps DK, 1981. Flat Dilatometer Manual. GPE Inc, Gainesville, Florida, USA.

Meyerhof GG, Adams JI, 1968. The ultimate uplift capacity of foundations. *Canadian Geotechnical Journal*, 5(4): 225-244. https://doi.org/10.1139/t68-024

Pacheco MP, Danziger FAB, Pinto CP, 2008. Design of shallow foundations under tensile loading for transmission line towers: an overview. *Engineering Geology*, 101(3-4):226-235. https://doi.org/10.1016/j.enggeo.2008.06.002

Park J, Qiu T, Kim Y, 2013. Field and laboratory investigation of pullout resistance of steel anchors in rock. *Journal of Geotechnical and Geoenvironmental Engineering*, 139(12):2219-2224. https://doi.org/10.1061/(ASCE)GT.1943-5606.0000953

Phoon KK, 2006. Modeling and simulation of stochastic data. GeoCongress 2006, p.1-17. https://doi.org/10.1061/40803(187)3

Qian ZZ, Lu XL, Tong RM, 2014. Uplift load–movement response of bell pier foundations in Gobi gravel. *Proceedings of the Institution of Civil Engineers-Geotechnical Engineering*, 167(4):380-389. https://doi.org/10.1680/geng.12.00072

Qian ZZ, Lu XL, Han X, et al., 2015. Interpretation of uplift load tests on belled piers in Gobi gravel. *Canadian Geotechnical Journal*, 52(7):992-998. https://doi.org/10.1139/cgj-2014-0075

Randolph MF, 1978. A Theoretical Study of the Performance of Piles. PhD Thesis, University of Cambridge, Cambridge, UK.

Serrano A, Olalla C, 1999. Tensile resistance of rock anchors. *International Journal of Rock Mechanics and Mining Sciences*, 36(4):449-474. https://doi.org/10.1016/S0148-9062(99)00021-2

Sun YZ, Pan K, Tang C, et al., 2022. Field experimental study on cyclic uplift behavior of anchored pier foundations. *Acta Geotechnica*, 17(10):4419-4434. https://doi.org/10.1007/s11440-022-01503-x

Tang C, Phoon KK, 2018. Statistics of model factors and consideration in reliability-based design of axially loaded helical piles. *Journal of Geotechnical and Geoenvironmental Engineering*, 144(8):04018050. https://doi.org/10.1061/(ASCE)GT.1943-5606.0001894

Wang G, Kasali G, Sitar N, 2011. Static and dynamic axial response of drilled piers. I: field tests. *Journal of Geotechnical and Geoenvironmental Engineering*, 137(12):1133-1142. https://doi.org/10.1061/(ASCE)GT.1943-5606.0000547

Wu WB, Yang ZJ, Liu X, et al., 2022. Horizontal dynamic response of pile in unsaturated soil considering its construction disturbance effect. *Ocean Engineering*, 245:110483. https://doi.org/10.1016/j.oceaneng.2021.110483

Zhang QQ, Feng RF, Xu ZH, et al., 2019. Evaluation of ultimate pullout capacity of anchor cables embedded in rock using a unified rupture shape model. *Geotechnical and Geological Engineering*, 37(4):2625-2637. https://doi.org/10.1007/s10706-018-00782-0

Zhang YP, Jiang GS, Wu WB, et al., 2022. Analytical solution for distributed torsional low strain integrity test for pipe pile. *International Journal for Numerical and Analytical Methods in Geomechanics*, 46(1):47-67. https://doi.org/10.1002/nag.3290

Electronic supplementary materials

Sections S1–S5, Videos S1 and S2